The use of ionospheric tomography and elevation masks to reduce the overall error in single-frequency GPS timing applications

Julian A. R. Rose[1], Jenna. R. Tong[2], Damien J. Allain[3], Cathryn N. Mitchell[4]

[1,2,3,4]*Invert Centre for Imaging Science, Department of Electronic and Electrical Engineering, University of Bath, Bath, BA2 7AY, UK*

[1]j.a.r.rose@bath.ac.uk
[2]j.r.tong@bath.ac.uk
[3]d.allain@bath.ac.uk
[4]c.n.mitchell@bath.ac.uk

Abstract

Signals from Global Positioning System (GPS) satellites at the horizon or at low elevations are often excluded from a GPS solution because they experience considerable ionospheric delays and multipath effects. Their exclusion can degrade the overall satellite geometry for the calculations, resulting in greater errors; an effect known as the Dilution of Precision (DOP). In contrast, signals from high elevation satellites experience less ionospheric delays and multipath effects. The aim is to find a balance in the choice of elevation mask, to reduce the propagation delays and multipath whilst maintaining good satellite geometry, and to use tomography to correct for the ionosphere and thus improve single-frequency GPS timing accuracy. GPS data, collected from a global network of dual-frequency GPS receivers, have been used to produce four GPS timing solutions, each with a different ionospheric compensation technique. One solution uses a 4D tomographic algorithm, Multi Instrument Data Analysis System (MIDAS), to compensate for the ionospheric delay. Maps of ionospheric electron density are produced and used to correct the single-frequency pseudorange observations. This method is compared to a dual-frequency solution and two other single-frequency solutions: one does not include any ionospheric compensation and the other uses the broadcast Klobuchar model. Data from the solar maximum year 2002 and October 2003 have been investigated to display results when the ionospheric delays are large and variable. The study focuses on Europe and results are produced for the chosen test site, VILL (Villafranca, Spain). The effects of excluding all of the GPS satellites below various elevation masks, ranging from 5° to 40°, on timing solutions for fixed (static) and mobile (moving) situations are presented. The greatest timing accuracies when using the fixed GPS receiver technique are obtained by using a 40° mask, rather than a 5° mask. The mobile GPS timing solutions are most accurate when satellites at lower elevations continue to be included: using a mask between 10° and 20°. MIDAS offers the most accurate and least variable single-frequency timing solution and accuracies to within 10 ns are achieved for fixed GPS receiver situations. Future improvements are anticipated by combining both GPS and Galileo data towards computing a timing solution.

Keywords

GPS; tomography; timing; ionosphere; satellite elevation.

1. Introduction

The Global Positioning System (GPS) may be used to provide timing information to users virtually anywhere in the world. Purpose built GPS timing receivers typically use a specific algorithm, that incorporates the receiver's fixed and known position coordinates, in order to provide timing information (Dana, 1997). When the receiver position is known, a timing solution may be obtained from just one GPS satellite. This however could lead to a highly unreliable solution, due to environmental, atmospheric and satellite specific errors. These receivers are not suited to a dynamic environment and contrastingly, navigation receivers must process signals from at least four GPS satellites in order to compute the user's 3D position and time. These are suited to fixed and mobile applications. However, any errors in the measurements used to estimate the position will propagate into the timing solution. If such receivers are to be used for timing purposes then improved accuracies (relative to fixed timing receivers) may be obtained when placed in a fixed position over time; allowing the positional solution to improve over averaging and smoothing times of a few hours or more. Both fixed and mobile receiver scenarios are considered in this paper and described later.

One of the largest error sources in a single-frequency GPS solution is due to the ionosphere (Langley, 1997) which both slows and refracts GPS signals as they propagate through it. This unknown propagation delay is highly variable and dependent upon several factors, such as: time of day, latitude, solar activity and season (Davies, 1990). The effect is proportional to the Total Electron Content (TEC), the line integral of the ionospheric electron density. The GPS satellites broadcast corrections for the ionosphere in the form of 8 coefficients via the navigation message. The coefficients represent a global model of the ionosphere, which was designed by Klobuchar (1987), and is used by standard single-frequency GPS receivers to correct for the ionosphere in real-time. Similarly, ionospheric correction coefficients will be broadcast via the Galileo navigation message, for single-frequency users (Hochegger et al., 2000). The International Reference Ionosphere (IRI) is another ionospheric model (Bilitza and Reinisch, 2008), but it is not available in real-time and is therefore not presented in the results. Future development of the NeQuick ionospheric model (Radicella and Leitinger, 2001) will provide an alternative to that of Klobuchar (1987). Further 2-D mapping techniques include those used by the: Wide Area Augmentation System (WAAS) (El-Arini et al., 1995), European Geostationary Navigation Overlay Service (EGNOS) (Hein, 2000) and Multi-functional Satellite Augmentation System (MSAS) (Matsunaga et al., 2003). These use geostationary satellite systems to broadcast real-time ionospheric mapping information to enhance the GPS solution for such capable GPS receivers.

This paper uses the Multi-Instrument Data Analysis System (MIDAS) (Mitchell and Spencer, 2003) algorithm to compensate for the ionospheric delay for single-frequency GPS systems. MIDAS is a 4D tomographic algorithm capable of mapping the ionosphere in three spatial dimensions and in real-time. It is used to provide the ionospheric delay by producing maps of electron density. Meggs and Mitchell (2006) and Smith et al. (2008) have demonstrated that such imaging techniques more accurately represent the ionosphere than 2D approximations. In order to track and monitor the time evolving plasma flow in the ionosphere (to produce 4D maps), a large network of GPS receivers is required over the desired region. This

infrastructure is already in place through the International GNSS (Global Navigation Satellite System) Service (IGS) (Dow et al., 2009) and the Regional Reference Frame Sub-Commission for Europe (EUREF) Permanent Network (EPN) (Bruyninx, 2004), making this possible over Europe and other parts of the world. Together they consist of hundreds of fixed GNSS stations that provide several GNSS products. This study focuses on Europe and it is important to note that the behaviour of the ionosphere varies according to geographic location. Solar tides and horizontal geomagnetic field lines dominate the evolution of the ionosphere at low latitudes. Electron precipitation and the solar wind govern the ionospheric dynamic at high latitudes (Mitchell et al., 2005), whereas at mid-latitudes, neutral winds and the inner magnetosphere drive the dynamics (Kintner et al., 2007).

Signals from GPS satellites at high elevations (or directly overhead at zenith) travel through smaller portions of the ionosphere on their journey towards Earth and so contribute smaller errors to the GPS solution, in contrast to signals from GPS satellites at low elevations (near the horizon). Low elevation signals travel through a larger part of the ionosphere, are subject to more multipath and are hence delayed by a larger and unknown amount when compared to high elevation signals. Satellite geometry plays an important role with respect to a GPS navigation/timing solution and may be measured by the Dilution of Precision (DOP). A good DOP is most likely to occur when there are wide angles of separation between the satellites, allowing more accurate horizontal and vertical positioning solutions, and hence timing solutions, to be found. A poor DOP is most likely when there are small angles of separation between the satellites. Overall, the future combination of the Galileo and GPS constellations will lead to greater performance, enhanced satellite geometry and a more dependable GNSS service (Feng, 2003). More signals and measurements will be available, resulting in more accurate GNSS solutions and could lead to improved ionospheric modelling techniques (Hernández-Pajares et al., 2003).

The satellite geometry is investigated by enforcing various elevation masks, which begin at 5° and increase in steps of 5° up until 40°. Masks beyond this value are not employed due to the limited number of satellites available above 40°. Signals from GPS satellites originating from below the value of the elevation mask are excluded from the solution. For a mobile GPS receiver, signals from both high and low elevation satellites are required to calculate a good positioning and hence timing solution. Therefore, there is a trade-off to be made between excluding extremely low elevation satellites whilst still including some in order to calculate an accurate position. In contrast and since fixed GPS receivers only require one GPS satellite to calculate a timing solution, signals from a high elevation satellite are desirable, as they would be expected to contribute less ionospheric and multipath errors into the solution. However, relying solely on one satellite can be hazardous due to environmental and atmospheric effects, not to mention potential satellite specific errors, which may be unknown for several hours. Typically therefore, GPS timing receivers depend upon several satellites towards producing a timing solution.

The aim is to minimise multipath, DOP and the ionospheric delay by finding a balance between the elevation mask and satellite geometry. Ionospheric tomography is also used towards producing a more accurate single-frequency GPS timing solution. In total, four separate GPS timing solutions are presented in the results, each with a different method of ionospheric compensation. The solutions are presented for fixed

and mobile GPS receivers with: no ionospheric correction, the Klobuchar model, MIDAS and dual-frequency corrections. The first three are single-frequency solutions. The solution with no correction illustrates the sheer magnitude of the ionospheric delay, whilst the Klobuchar solution demonstrates the current capability of single-frequency receivers. The 4D tomographic real-time mapping system, MIDAS, portrays the capability of an ionospheric tomography system. The dual-frequency solution provides a direct means of measuring the first order ionospheric delay and is hence a benchmark solution.

2. Method

2.1 Overview

This paper builds upon the techniques described by Rose et al. (2009) to investigate the relationship between satellite geometry and GPS timing accuracy. Ionospheric tomography and elevation masks are the key focus points. Results are presented for fixed and mobile receiver situations. Allain and Mitchell (2009) use similar techniques to investigate the relationship between various ionospheric models and GPS positioning.

Geophysically quiet and stormy days from the year 2002 and a stormy period in October 2003 have been included in this study in order to represent diverse geophysical conditions. As GPS signals propagate through the ionosphere during 'quiet' periods such as solar minimum (a period of reduced ionospheric activity) they are delayed by smaller amounts. This is in contrast to periods of high ionospheric activity, which is more common during solar maximum conditions and can lead to significant delays upon GPS signals. It is relevant to present results during both quiet and stormy conditions because they are both equally valid situations. Furthermore, it is important to illustrate the performance of MIDAS under challenging geophysical conditions. Days were chosen according to the Kp index, which measures the disturbances in the Earth's magnetic field and ranges from 0-9. Quiet and stormy days are represented by values between 0-4 and 5-9 respectively. It is important not to depend solely upon the Kp index to indicate the local geophysical conditions, but simply to use it as a general indication that a higher Kp is more likely to correspond to an enhancement in the ionosphere, but perhaps not over the particular area of interest. TEC maps may be plotted over these areas to illustrate the local ionospheric activity. The Kp data are provided by the World Data Center for Solar Terrestrial Physics and downloaded from the UK Solar System Data Centre (UKSSDC) http://www.ukssdc.ac.uk/.

Collectively, data from 74 IGS (Dow et al., 2009) and EPN (Bruyninx, 2004) sites across mainland Europe are used in this study. These, together with MIDAS, are used to create 4D real-time ionospheric maps, which are then employed to mitigate the ionospheric delay imposed upon the GPS signals. The tomographic grid ranges from -44° to +44° in steps of 4° in longitude and latitude and is centered on Europe at 50°N 15°E (see Figure 1). The altitude ranges from 100 km to 1500 km in steps of 50 km. MIDAS uses three empirical orthonormal functions to represent the vertical basis

functions, which are computed from a breadth of Epstein functions. Please see Mitchell and Spencer (2003) and Spencer and Mitchell (2007) for more detailed information.

An additional IGS station was chosen as a test site; VILL (Villafranca, Spain). This data does not contribute to the ionospheric mapping since independent timing solutions are desired. The data from the test site are used to demonstrate the performance of a single-frequency GPS receiver with: no ionospheric correction, the Klobuchar ionospheric correction and finally the MIDAS correction. Dual-frequency data are included in the resulting figures to enable direct comparisons between various GPS timing solutions.

2.2 The GPS timing solution

Data from the 74 dual-frequency GPS receiver sites located across mainland Europe have been obtained in Receiver Independent Exchange (RINEX) format (Gurtner, 2002) from the IGS/EPN. These data are used towards computing GPS timing solutions. The GPS satellites are synchronised to GPS Time (GPST) and their positions are calculated using the precise ephemerides, which are provided by the IGS. The local Time of Arrival (TOA) is recorded by a GPS receiver (according to its clock) at the time of reception of a GPS signal. The time at which the satellite broadcast the signal, the Time of Transmission (TOT) is incorporated within the navigation message. Therefore, the pseudorange between each GPS satellite and the receiver may be computed. The pseudorange may be defined as the difference between the satellite clock time and the receiver clock time (Parkinson and Spilker, 1996). This is corrupted by the receiver clock bias, which must be estimated and removed from the solution and is denoted by RCB from this point on. Various other biases and propagation errors are imposed upon the GPS signals and the system as a whole and so a number of corrections are applied to the pseudorange equations, before the specific ionospheric corrections, that are fundamental and common to each of the GPS timing solutions presented in this research. The pseudorange equation and corrections are explained shortly.

The RCB is the offset between the GPS receiver's clock and GPST. The following describes the methods used to obtain the RCB for both fixed and mobile receiver situations. In the case of the fixed receiver, whereby the receiver's position is known, the common and fundamental corrections are calculated and applied to the solution from the outset. These are explained shortly and include biases such as the: Sagnac bias, tropospheric delay and satellite specific biases. The RCB is then obtained by averaging all of the RCB values for all of the satellites in view at each instant in time. Of course, when the receiver position is known the RCB may be found from just one satellite, however this would lead to a highly unreliable solution. In the case of the mobile receiver, when the receiver's position is unknown, at least four GPS satellites are required to solve for the position and RCB. If four satellites are being tracked, then four pseudorange equations are formed to solve for x, y, z and b_{rx} (the RCB) using a least squares technique described by Rose et al. (2009). Initial estimates for the common and fundamental corrections are formed using an approximation of the receiver coordinates. This is an iterative technique that begins with a fairly rough approximation of the receiver's position and clock bias, and results

in more and more accurate x, y, z and b_{rx} values. Note that if there are less than 4 satellites in view, due to the enforcement of a high elevation mask perhaps, the mobile GPS timing solution presented here will fail. This method is used to demonstrate that high elevation masks are not suited to mobile GPS receiver applications, albeit that in reality if less than 4 satellites are in view GPS receivers may have some memory of their previous position and so may be able to continue providing a solution for a short while, however, as time passes, the more degraded and unreliable the solution would become. Incidentally, the combination of the Galileo and GPS constellations will make more satellites available at higher elevations at any given time.

Once the RCB has been resolved, the GPST at the receiver is known. Note that the GPST may be converted to Coordinated Universal Time (UTC) using the specific conversion parameter broadcast in the GPS navigation message; however, this is not implemented in this study. Each of the timing solutions presented here employ these techniques (depending upon scenario: fixed or mobile) and the common/fundamental corrections; only the method by which the ionospheric delay is accounted for separates them. Each type of timing solution yields the RCB at the receiver, which is presented relative to the precise bias as calculated by the Centre for Orbit Determination in Europe (CODE). This is an IGS Analysis Center that uses the GPS code and phase measurements, along with atomic clock references to calculate their clock solutions (Kouba and Springer, 2001) and is taken as a reference solution to give a fair and independent comparison between methods. The offset between the timing solutions presented in the results, at VILL, and the solution provided by the CODE is due to differences in filtering to remove multipath: the CODE solution is obtained using integer ambiguity resolution, whereas the presented timing solutions are obtained using phase filtering only (Rose et al., 2009). Ambiguity filtering is not used because it is not feasible for the timing methods presented in this paper. The integer ambiguity is constant as long as the received power is sufficient. The presented timing solutions, for both the fixed and mobile cases, are calculated instantaneously at each sampling point, without relying on historic or averaged data and produce a solution without prior knowledge of the local multipath effects. The phase filtering yields the sum of the integer ambiguity and of the small multipath average, offering improvements over raw multipath error and noise. The offset is location/site specific and in the case of GPS, is repeated every sidereal day.

2.3 Pseudorange and common corrections

These corrections are fully described by Rose et al. (2009). The difference between the receiver clock time (TOA), t_r and the satellite clock time (TOT), t_t yields the pseudorange, P (in seconds) but it is corrupted by several other factors:

$$P = (t_r - t_t) + b_{rx} + b_{sv} + T_{sagn} + T_{trop} + T_{iono} + \varepsilon \qquad (1)$$

The RCB is the receiver's clock offset from GPST and is represented by b_{rx}. The satellite clock bias, b_{sv} accounts for the satellite specific error and the satellite relativistic effects. The Sagnac bias, T_{sagn} accounts for the Earth's rotation during the propagation time of the GPS signal. T_{trop} represents the error imposed upon the GPS signal as it propagates through the troposphere. T_{iono} represents the delay due to the ionosphere and is mitigated using different techniques which are later described. Any unmodeled errors are represented by ε and are ignored.

2.4 Fundamental corrections and calculations

In order to compute the GPS solution the following corrections are necessary, which are implemented and fully described by Rose et al. (2009). The precise ephemerides were obtained from the IGS and used to calculate the satellite positions. There is a small offset between the single-frequency and dual-frequency clock biases, known as the Differential Code Bias (DCB), which is given in the ephemeris data. The two codes, modulated onto the L1 and L2 frequencies, have finite electrical path lengths at the transmitter and receiver, resulting in a small P1 to P2 bias - a different clock bias for each frequency. The DCB are satellite and receiver specific and are provided by the CODE. The dual-frequency clock bias is contained within the IGS ephemeris and so the single-frequency clock bias is offset from the dual-frequency clock bias and is corrected. The ephemeris data are calculated with respect to the satellite's centre of mass as opposed to signal measurements, which are relative to the Antenna Phase Center (APC) and so these antenna offsets must also be corrected for. Trigonometric interpolation is used to obtain the antenna coordinates at the TOT from the ephemeris (with the antenna offsets applied). Iterative methods are used to extract the TOT, provided the TOA and range between satellite and receiver are known, or at least approximated. The satellite velocities are hence found and used, together with the precise satellite positions, to calculate the Sagnac bias and the relativistic satellite clock biases.

A set of partially corrected pseudorange equations for each satellite-to-receiver ray path results from the application of the fundamental and common corrections, which forms the foundation for each GPS timing solution. The ionospheric delay remains the only effect to be accounted for.

2.5 Ionospheric corrections

Part of this research focuses on using tomography to mitigate the ionospheric delay in single-frequency GPS timing applications. In total, four timing solutions are presented in the results, each of which employs a different method of ionospheric compensation and are fully described by Rose et al. (2009). The P1 code is extracted from the RINEX file to form the solution with no ionospheric correction. This illustrates the diurnal effect of the ionosphere and its impact on GPS timing accuracy. Following that, the current ability of standard single-frequency GPS receivers is portrayed by the timing solution that incorporates the Klobuchar model for ionospheric correction (Klobuchar, 1987). Eight coefficients are broadcast via the GPS navigation message to represent this global model of the ionosphere. In general a minimum of 50% Root Mean Square (RMS) correction is achieved. MIDAS, coupled with the pure single-frequency solution was presented by Rose et al. (2009) and uses data from the IGS/EPN network to produce 4D real-time ionospheric maps. The ionospheric (group) delay may be found as follows:

$$T_{iono} = \frac{40.3}{cf^2} \int Ndl \qquad (2)$$

where c is the speed of light, f is the frequency of the GPS signal (L1, 1575.42 MHz) and $\int Ndl$ is the TEC in electrons per squared metre. The line integral of the electron

density between the satellite-to-receiver ray-path is provided by MIDAS to yield the TEC. The ionosphere-free pseudorange, denoted by P0 here, is used to calculate the dual-frequency solution. Four observables, P1 and P2 (which represent the pseudoranges from the precise P-code signal) and L1 and L2 (the recorded carrier phases of the signal in terms of distance) are used to compute P0. This solution acts as a benchmark because it is widely considered to be the best ionospheric compensation technique, provided that accurate DCB are obtained. This is because it uses two GPS signals (at different frequencies) to measure the ionospheric delay.

2.6 Multipath

Various elevation masks are employed with the aim of limiting multipath, but whilst maintaining reasonably good satellite geometry for the calculations. It is beyond the scope of this paper to focus on techniques that attempt to significantly remove multipath from a GPS solution. In precise GNSS applications, and due to reflections from the local environment, multipath may be considered as one of the most limiting factors (Axelrad et al., 1996). Multipath is the same from one sidereal day (23 h 56 m 04 s) to the next, due to the repeatability of the GPS satellite ground-tracks (Choi et al., 2004). Sidereal filtering takes advantage of this repetition and may be used to help reduce the errors due to multipath in GNSS solutions (Ragheb et al., 2007). For sidereal filtering, data is required from at least two consecutive orbits. Following the estimation of 1 Hz positions for day one, high-frequency noise (unrelated to the satellite-receiver geometry) is removed via a low-pass filter. These positions are then shifted by the sidereal period and subtracted from the estimated positions on the second day (Choi et al., 2004). Multipath may be identified in the results by analysing the GPS timing accuracies over consecutive days: if there is a significant error in timing accuracy, due to multipath, on one particular day then it should also be evident the following sidereal day.

2.7 Satellite Geometry and DOP

GPS satellite positions may be described by azimuth and elevation angles, which are important when investigating the relationship between satellite geometry and GPS timing accuracy. The elevation angles at the horizon and at zenith are 0° and 90° respectively. North, East, South and West are represented by azimuth angles of 0°, 90°, 180° and 270° respectively. The ranging accuracy, multiplied by a dilution factor (that depends solely on geometry) may be used to estimate the positioning accuracy (Parkinson and Spilker, 1996).

The number of GPS satellites in view also plays an important role; the more satellites there are, the more likely a good DOP will be obtained. The Position DOP (PDOP) gives a measure of the positioning accuracy (vertical and horizontal), while more specifically, the Horizontal and Vertical DOP are measured by the HDOP and VDOP respectively. Time DOP (TDOP) may be used as an indicator of timing accuracy and the Geometric DOP (GDOP) includes PDOP and TDOP. In general, a DOP greater than 6 represents poor satellite geometry and the worldwide PDOP median is roughly 2.5 according to Parkinson and Spilker (1996). The satellite geometry directly impacts the accuracy of the horizontal and vertical positioning solutions. The vertical positioning errors are correlated with the timing errors (explained below) and are therefore presented in the results, along with the TDOP.

The following shows the relationship between the satellite geometry and the positioning error (Parkinson and Spilker, 1996):

$$\Delta\bar{\boldsymbol{x}} = \boldsymbol{G}^{-1}\Delta\bar{\rho}_c \qquad (3)$$

where $\Delta\bar{\boldsymbol{x}}$ is the positioning error, $\boldsymbol{G}$ is the geometry matrix and $\Delta\bar{\rho}_c$ represents the pseudorange errors to each satellite. The satellite elevation and azimuth angles θ and ϕ respectively, can be translated into the east, north, up coordinate frame. The geometry matrix, for four satellites, is shown below:

$$\mathrm{G} = \begin{bmatrix} \cos\theta_1 \sin\phi_1 & \cos\theta_1 \sin\phi_1 & \sin\theta_1 & 1 \\ \cos\theta_2 \sin\phi_2 & \cos\theta_2 \sin\phi_2 & \sin\theta_2 & 1 \\ \cos\theta_3 \sin\phi_3 & \cos\theta_3 \sin\phi_3 & \sin\theta_3 & 1 \\ \cos\theta_4 \sin\phi_4 & \cos\theta_4 \sin\phi_4 & \sin\theta_4 & 1 \end{bmatrix} \qquad (4)$$

The covariance matrix of the solution may be expressed as follows (in m^2):

$$\mathrm{cov}(solution) = \sigma_R^2 \begin{bmatrix} (EDOP)^2 & & & \\ & (NDOP)^2 & & \\ & & (VDOP)^2 & \\ & & & (TDOP)^2 \end{bmatrix} \qquad (5)$$

where σ_R^2 is the variance, EDOP and NDOP are the East and North DOP respectively, which make up the HDOP. The GDOP is the square root of the trace of the GDOP matrix and may be found as follows:

$$GDOP = \sqrt{(EDOP)^2 + (NDOP)^2 + (VDOP)^2 + (TDOP)^2} \qquad (6)$$

Negative correlation between vertical positioning errors and timing errors are shown by an example in Parkinson and Spilker (1996) that yields non-zero off diagonal terms in the covariance of position matrix. Accordingly, a positive timing error will typically correspond with a negative vertical positioning error and vice versa. In general, vertical positioning and timing errors largely correlate and with opposite signs.

2.8 Elevation Masks

An elevation mask of 20° means that signals from all of the GPS satellites below this value will be ignored and only signals from those above it will be included in the timing solution. The masks range from 5° to 40° in steps of 5°. Lower elevation masks are most likely to yield better DOP's than high elevation masks. This is because there are fewer satellites in view at higher elevations, which reduces the likelihood of good angles of separations between them. High elevation satellite

signals are less prone to multipath and ionospheric delays in comparison to signals originating from low elevation satellites. GPS satellite elevation angles are linked to multipath (Jin and de Jong, 1996), whereas satellite azimuth angles are not crucial to this investigation, but may aid towards specifically locating multipath sources if desired.

3. Results

GPS timing solutions for fixed and mobile GPS receiver situations are presented that employ various elevation masks and different ionospheric compensation techniques. The figure titles specify the: receiver name, date(s), type of solution (fixed/mobile, where relevant) and elevation mask. The figure captions include the minimum and maximum Kp indices measured for the particular period. These results are representative of solar maximum conditions.

Figures 2a-c represent the diurnal variation in RCB for 13 February 2002, at VILL, using the *fixed* receiver solution. A dashed horizontal line is fixed at 80 ns RCB to help compare the reduction in the diurnal peak of RCB when using a 20° or 40° elevation mask, as opposed to a 10° mask. These figures imply that the accuracy of a GPS timing solution, for a *fixed* receiver, improves as satellites at lower elevations are excluded. The 'no correction' curves effectively illustrate the magnitude of the ionospheric error and this clearly reduces as the elevation mask increases from 10° to 40°: the curve peaks at approximately 80 ns in Fig. 2a and at roughly 55 ns in Fig. 2c respectively. Table 1 summarizes the RMS RCB for both the geophysically quiet and stormy days selected from 2002, at VILL (using the fixed solution). The data includes one quiet and stormy day from each month, excluding September due to data quality. Table 2 summarizes the standard deviations over the same period. According to Table 1, the most accurate solutions are obtained by employing the highest elevation mask tested, 40°, as opposed to the lowest elevation mask, 5°. By comparing these masks, the greatest improvements in timing accuracy are shown by the no correction and Klobuchar solutions: 30% and 29% respectively. The MIDAS and dual-frequency timing solutions improve by only 9% and 5% respectively under the same circumstances. These reductions are most likely due to both the decrease in propagation delay and multipath when using the 40° mask. Overall, Table 2 indicates that the higher the elevation mask, the less variable the timing solution becomes. This table shows that the timing solution with no ionospheric correction has a standard deviation of 13.1 ns when an elevation mask of 15° is employed. This solution improves by 26% when a 40° mask is used. The Klobuchar solution is shown to be less variable and improves by 20% when using a 40° mask as opposed to a 15° mask. The MIDAS and dual-frequency solutions have lower and similar standard deviations than the other solutions, so much so that the changes in elevation mask have little effect. In fact, one would expect that as the elevation mask is increased, the dual-frequency solution would become less variable. This is true when comparing only the 40° mask with the 5° mask, however the standard deviations for the 15° and 20° mask are both 0.2 ns higher than the standard deviation obtained using a 5° mask. Though these changes are relatively small, it does suggest that there are other accuracy-limiting factors such as multipath.

Figure 3a shows the diurnal variation in RCB for 13 February 2002, at VILL, using the *mobile* receiver solution and an elevation mask of 20°. Figures 3b-e are presented to explain particular anomalies. Figures 3b and 5b illustrate the number of satellites in view and the TDOP. A dotted horizontal line marks the threshold at which there are only 4 satellites in view. When the number of satellites falls below this threshold, the corresponding mobile timing solution is unavailable because at least 4 satellites are required for a 4D solution. Two prominent examples of error in the timing solution are shown at approximately 04:00 UT h and 20:00 UT h (see the large spikes) in Fig. 3a. Figure 3b shows that just before 04:00 UT h the number of satellites in view dropped from 6 to 5, which was followed by an increase in the TDOP. Additionally, just before 20:00 UT h, the number of satellites in view momentarily dropped from 5 to 3 (see the slight data gap in Fig. 3a) before settling at 4 in view, which is accompanied by a rise in TDOP. Figures 3c and 5c show the satellite elevation angles of all of the satellites in view on the day in question, each curve represents a particular satellite. A dashed horizontal line has been placed at the satellite elevation angle of 20° on Fig. 3c. The satellite tracks above/below this line represent those that are available/unavailable when a 20° elevation mask is implemented. The dashed vertical lines in Figures 3c and 5c highlight particular periods of interest, whilst the green patches illustrate instances when only satellites at high elevations are available (around 30-40° for example). For the purpose of this investigation, it is not necessary to show which curve corresponds to which GPS satellite. Figure 3c shows that at around 04:00 UT h and above 20° elevation, there is a period when only satellites at even higher elevations were available. This is akin to an even higher elevation mask that varies between ~20° and ~40°. Figures 3d and 3e show that the vertical positioning errors are much larger than the horizontal positioning errors. By analysing the no correction curves: the midday peak in vertical positioning error reaches approximately -28 m, which is equivalent to roughly 93 ns and the midday peak in RCB is roughly +112 ns (see Fig. 3a). This agrees with the relationship explained in the Method (see section 2.7), whereby the vertical positioning errors are most likely to correlate with the timing errors and with opposite signs.

Figure 4a shows the variation in RCB using a 20° mask over a consecutive three day period, 13-15 February 2002 inclusive. A dashed vertical line is shown to represent the boundary line between each consecutive day. The previously discussed anomalies from Fig. 3a are now of course evident in the first day shown in Fig. 4a and are repeated on the following two days. See the spikes at around 04:00 and 20:00 UT h. By analysing these consecutive days, the most likely cause of the anomalies is due to the satellite geometry. More specifically, as the number of satellites in view decreases there is a reduced likelihood of a good DOP, as is the case here, whereby only high elevation satellites are in view. This prevents an accurate positioning solution from being calculated, which in turn causes a large TDOP and results in a degraded timing solution. Similarly, distinctive anomalies exist at around 11:00, 12:00 and 13:00 UT h for the 14 and 15 February 2002 in Fig. 4a (see the large spikes). They are also evident for 13 February 2002, though on a smaller scale. Fig. 3b shows that at these times the TDOP increases significantly and the number of satellites in view changes rapidly at around 11:00 to 12:00 UT h and fluctuates between 6 and 5 at 13:00 UT h. Figure 4b shows the variation in RCB using a 10° mask over the same period. By comparing Figures 4a and 4b, the single-frequency solutions show less variability in Fig. 4a (20° mask) when compared to Fig. 4b (10°

mask), most notably from midday onwards. The dual-frequency solution however becomes more variable. Furthermore, there are more anomalies when using a 20° elevation mask, rather than the 10° mask. This indicates that there is a trade-off between the size of the elevation mask and the timing accuracy. When the elevation mask is too high, there is a bad effect on satellite geometry and TDOP (see Fig. 3b-c).

The single-frequency and even the dual-frequency solutions exhibit a clear anomaly between ~03:00 and ~04:00 UT h in Fig. 5a. Figure 5c illustrates that the most likely cause is due to a lack of GPS satellites between 0° and ~40° elevation at particular instances during this period (see highlighted area). Figure 5b shows that at this time the number of satellites in view drops to 6 and there is an increase in TDOP. Large increases in TDOP at 11:00 and 14:00 UT h coincide with setting satellites and correspond to slight anomalies in Fig. 5a at these times (see the small downward spikes).

Figure 6a shows the variation in RCB (using a 15° mask and the fixed timing solution) over a consecutive five day period, 27-31 October 2003 inclusive. Two Coronal Mass Ejections (CME) were detected on days 302 and 303, which led to global and intense geomagnetic storms. These two days mark the positive and negative phases of the storm respectively, across the European region. A snapshot of the ionosphere across Europe on the 29 October 2003 (day 302) at 19:00 UT h is shown by Fig. 6b. This figure was produced using MIDAS and shows the spatial distribution of vertical TEC. TEC Units ranging between 40-60 are apparent across VILL at this time and correspond to the highly variable peak in RCB, which continues deep into the night, shown by the no correction curve in Fig. 6a. The negative phase of the storm causes a depression in the ionosphere, resulting in the lower than average RCB for the curve with no correction on day 303 (Fig. 6a). Table 3 summarizes the RMS RCB for 27-31 October 2003, at VILL (using the fixed solution). Table 4 summarizes the standard deviations over the same period. According to Table 3, the most accurate solutions are achieved when the highest elevation mask (40°) is employed. Notably the no correction and Klobuchar RMS RCB values differ by less than 3 ns, whichever mask is used. The latter solution performs only slightly better. The MIDAS and dual-frequency RMS RCB values are comparable, differing by less than 2 ns irrespective of elevation mask. Table 4 shows that the no correction and Klobuchar solutions are least variable when the highest elevation mask is used. The variability of the MIDAS and dual-frequency solutions remains largely constant irrespective of elevation mask. Interestingly, Table 4 shows that the Klobuchar solution is roughly 32-36% more variable than the solution with no ionospheric correction, whichever elevation mask is used. This along with Fig. 6a (see days 300, 303 and 304) show that during intense geomagnetic storms it may be better not to employ the broadcast Klobuchar corrections. According to Table 4, and with a 15° mask, the standard deviations of the RCB for the MIDAS and dual-frequency solutions are 1.6 ns and 0.8 ns respectively. MIDAS and the dual-frequency solutions yield a 90% and 95% improvement respectively when compared to the Klobuchar solution.

4. Conclusions and Discussion

Ionospheric tomography and elevation masks have been used to reduce the overall timing error and produce a new single-frequency GPS timing solution. This is compared to other timing solutions produced for the IGS station, VILL (Spain) using fixed and mobile based receiver techniques. Results were produced using data from the previous solar maximum in 2002 and a particular stormy period in October 2003.

The tomographic mapping system, MIDAS, provides the most accurate and least variable single-frequency GPS timing solutions. Using MIDAS, accuracies to within 10 ns are achievable in fixed GPS receiver situations, even during periods of intense geomagnetic activity. In general and in increasing order the timing accuracy is as follows: no correction, Klobuchar, MIDAS and dual-frequency. However, during intense storms the Klobuchar solution may produce a worse timing solution than if there were no ionospheric correction at all. The method of ionospheric error compensation is integral to an accurate timing solution.

This research indicates that for fixed GPS receivers, the greater the elevation mask; the less variable and more accurate the timing solution will be. This relationship continues up to and including the 40° elevation mask, (masks beyond 40° have not been tested). This is because signals from satellites at high elevations are typically subject to less multipath and less ionospheric delays. Good satellite geometry is not crucial to a fixed timing solution and a balance between the number of available satellites and those at high elevations should be found. On the other hand, an elevation mask of 40° typically reduces the number of satellites in view to around 2 or 3 at any given time and since the average of all of the RCB's (calculated from all of the satellites in view) forms the fixed GPS timing solution, if just one of the satellites used is subject to a fault/error then it has the potential to seriously degrade the overall solution. Relying on just one satellite, or too few, can make it difficult to detect and remove satellite specific errors. Therefore, it would be prudent to employ some sort of warning/alarm system that could detect large anomalies and not only prevent the erroneous satellite from being included in the solution but also dynamically lower the elevation mask to increase the number of satellites in view. In continuation, a potential solution to this might be to perform TDOP analyses. By using the known receiver position (or trajectory of a mobile receiver) along with the satellite ephemeris data, the covariance matrix (from which the TDOP is calculated) may be computed prior to the actual data collection. This technique may be employed to give an advanced warning of the potential degradation in timing accuracy that could be due to changes in satellite geometry.

For mobile GPS receivers (unknown position) the timing solutions improve as the elevation mask is increased from 5° to 10°. Multipath appears to be reduced by using at least a 10° elevation mask. However, as the mask is increased from 10° to 20° some errors can be exasperated, due to the degradation of satellite geometry, that actually worsen the overall solution (whereas errors due to multipath and the ionosphere are expected to decrease with higher elevation mask). The best choice of elevation mask for a mobile receiver lies between: 10° and 20°. Nonetheless, even a 20° elevation mask can lead to times when there are less than 4 satellites in view. Although it may be crude to assume that as soon as there are less than 4 satellites are in view, the mobile GPS timing solution will fail; this method does suitably

demonstrate that high elevation masks are not suited to mobile GPS receiver applications. There are occasions when there are not any low elevation satellites in view at all, say between 0° and 40°. These periods have been shown to adversely affect the mobile timing solution. A balance must be struck between elevation mask and its effect on satellite geometry to minimise the propagation delays and optimise the timing solution, depending upon application. The rising/setting of satellites can worsen/improve the overall geometry, but the effects of acquiring/losing a satellite signal can lead to momentary fluctuations in timing accuracy and increases in TDOP.

The Galileo constellation will consist of 30 satellites and several new signals. These, together with the GPS constellation (and its forthcoming modernization) will lead to a much larger number of satellites in view at any given time and will improve the overall satellite geometry. This will result in a more dependable and reliable GNSS era, leading to improvements in positioning and timing accuracies. Please see http://www.esa.int/esaNA/galileo.html for more information. MIDAS is currently used to generate real-time ionospheric corrections, which are available via the internet. The corrections are created using GPS data, which are available from an existing infrastructure and are processed at the University of Bath. The corrections could be broadcast to actual GPS end-users in the field, in real-time, using a radio signal. This would enable more accurate GPS timing solutions to be obtained from a low-cost single-frequency GPS receiver, than is currently possible using the broadcast ionospheric corrections, albeit with a modification to enable them to receive and interpret the MIDAS data. It is intended that these real-time ionospheric corrections, for Europe, will be broadcast across the UK in the near future. Cosmic ray detectors, wired/wireless telecommunications systems and power transmission systems are just a few examples of applications that require accurate timing/synchronisation information. Two or more free running devices may be synchronised anywhere in the world, using GPS, to within 10 ns using the MIDAS system proposed here. This system could also help to reduce the risks of poor synchronisation during highly variable ionospheric conditions and in particular during the impending solar maximum.

Acknowledgments

We are very grateful to the UK Engineering and Physical Sciences Research Council (EPSRC) for funding this project and the IGS and EUREF for the GPS data, the GPS ephemeris and receiver clock products and the UKSSDC for the Kp data. We also wish to thank Nathan Smith (University of Bath) for his support. CNM also thanks the Royal Society for the Wolfson Research Merit Award.

References

Allain, D.J. and Mitchell, C.N. Ionospheric delay corrections for single-frequency GPS receivers over Europe using tomographic mapping. GPS Solut. 13(2), 141-151, 2009.

Axelrad, P., Comp, C.J. and Macdoran, P.F. SNR-based multipath error correction for GPS differential phase. IEEE Trans Aerosp. and Electron. Syst. 32(2), 650-660, 1996.

Bilitza, D. and Reinisch, B.W. International reference ionosphere 2007: Improvements and new parameters. Adv. Space Res. 42(4), 599-609, 2008.

Bruyninx, C. The EUREF Permanent Network: a multi-disciplinary network serving surveyors as well as scientists. GeoInformatics. 7, 32-35, 2004.

Choi, K., Bilich, A., Larson, K.M. and Axelrad, P. Modified sidereal filtering: Implications for high-rate GPS positioning. Geophys. Res. Lett. 31, 22, 2004.

Dana, P.H. Global Positioning System (GPS) Time Dissemination for Real-Time Applications. Real-Time Syst. 12(1), 9-40, 1997.

Davies, K. Ionospheric Radio, IEE Electromagnetic Waves, Peter Peregrinus Ltd., London, U.K., 1990.

Dow, J.M., Neilan, R.E. and Rizos, C. The International GNSS Service in a changing landscape of Global Navigation Satellite Systems. J Geod. 83(3), 191-198, 2009.

El-Arini, M.B., Conker, R.S., Albertson, T.W., Reagan, J.K., Klobuchar, J.A. and Doherty, P.H. Comparison of real-time ionospheric algorithms for a GPS Wide-Area Augmentation System(WAAS). J. Inst. Navig. 41(4), 393-413, 1995.

Feng, Y. Combined galileo and GPS: a technical perspective. J. Glob. Position. Syst. 2(1), 67-72, 2003.

Gurtner, W. RINEX: The Receiver Independent Exchange Format Version 2.10. Bull Am Meteorol Soc. 77, 1-18, 2002.

Hein, G.W. From GPS and GLONASS via EGNOS to Galileo – Positioning and Navigation in the Third Millennium. GPS Solut. 3(4), 39-47, 2000.

Hernández-Pajares, M., Zornoza, J.M.J., Subirana, J.S. and Colombo, O.L. Feasibility of wide-area subdecimeter navigation with GALILEO and Modernized GPS. IEEE Trans. Geosci. Remote Sens. 41(9), 2128-2131, 2003.

Hochegger, G., Nava, B., Radicella, S. and Leitinger, R. A family of ionospheric models for different uses. Phys. Chem. Earth. 25(4), 307-310, 2000.

Jin, X.X. and de Jong, C.D. Relationship between satellite elevation and precision of GPS code observations. J. Inst. Navig. 49(2), 253-265, 1996.

Kintner, P.M., Ledvina, B.M. and de Paula, E.R. GPS and ionospheric scintillations. Space Weather. 5(9), S09003, 2007.

Klobuchar, J.A. Ionospheric time-delay algorithm for single-frequency GPS users. IEEE Trans. Aerosp. Electron. Syst. 23(3), 325-331, 1987.

Kouba, J. and Springer, T. New IGS Station and Satellite Clock Combination. GPS Solut. 4(4), 31-36, 2001.

Langley, R.B. The GPS Error Budget. GPS World. 8(3), 51-56, 1997.

Matsunaga, K., Hoshinoo, K. and Igarashi, K. Observations of ionospheric scintillation on GPS signals in Japan. J. Inst. Navig. 50(1), 1-7, 2003.

Meggs, R.W. and Mitchell, C.N. A study into the errors in vertical total electron content mapping using GPS data. Radio Sci. 41(1) 2006.

Mitchell, C.N. and Spencer, P.S.J. A three-dimensional time-dependent algorithm for ionospheric imaging using GPS. Ann. Geophys. 46(4), 687-696, 2003.
Mitchell, C.N., Alfonsi, L., De Franceschi, G., Lester, M., Romano, V. and Wernik, A.W. GPS TEC and scintillation measurements from the polar ionosphere during the October 2003 storm. Geophys. Res. Lett. 32(12), L12S03, 2005.
Parkinson, B.W. and Spilker, J.J. Global Positioning System: Theory and Applications, vol 1, AIAA, 1996.
Radicella, S.M. and Leitinger, R. The evolution of the DGR approach to model electron density profiles. Adv. Space Res. 27(1), 35-40, 2001.
Ragheb, A., Clarke, P. and Edwards, S. GPS sidereal filtering: coordinate- and carrier-phase-level strategies. J Geod. 81(5), 325-335, 2007.
Rose, J.A.R., Allain, D.J. and Mitchell, C.N. Reduction in the ionospheric error for a single-frequency GPS timing solution using tomography. Ann. Geophys. 52(5), 469-486, 2009.
Smith, D.A., Araujo-Pradere, E.A., Minter, C.F. and Fuller-Rowell, T.J. A comprehensive evaluation of the errors inherent in the use of a two-dimensional shell for modeling the ionosphere. Radio Sci. 43, RS6008, 2008.
Spencer, P.S.J. and Mitchell, C.N. Imaging of fast moving electron-density structures in the polar cap. Ann. Geophys. 50(3), 427-434, 2007.

Fig. 1 Map of Europe, showing the test station VILL and those used for the inversion

Fig. 2a-c Receiver clock bias referenced to the receiver clock bias from CODE for VILL 13 February 2002 (Kp index 1.0-3.7) using a fixed receiver solution at an elevation mask of **(a)** 10° **(b)** 20° **(c)** 40°. Dashed horizontal line at 80 ns aids the comparison between elevation masks

Fig. 3a-e Various results for 13 February 2002, at VILL, using a mobile receiver solution and an elevation mask of 20° (Kp index 1.0-3.7), as follows: **(a)** Receiver clock bias referenced to the receiver clock bias from CODE, **(b)** the number of satellites in view and the TDOP, **(c)** the satellite elevation angles (the vertical dashed lines highlight the time periods of interest and the patches define the area more specifically), **(d)** the vertical positioning errors, **(e)** the horizontal positioning errors

Fig. 4a-b Receiver clock bias referenced to the receiver clock bias from CODE for VILL 13-15 February 2002 (Kp index 0-3.7) using a mobile receiver solution at an elevation mask **(a)** 20° **(b)** 10°

Fig. 5a-c Various results for 27 December 2002, at VILL, using a mobile receiver solution and an elevation mask of 5° (Kp index 3.3-6.0), as follows: **(a)** Receiver clock bias referenced to the receiver clock bias from CODE, **(b)** the number of satellites in view and the TDOP, **(c)** the satellite elevation angles (the vertical dashed lines highlight the time periods of interest and the patch defines the area more specifically)

Fig. 6a-b Results for October 2003: **(a)** Receiver clock bias referenced to the receiver clock bias from CODE for VILL 27-31 October 2003 (Kp index 1.0-9.0) using a fixed receiver solution at an elevation mask of 15°, **(b)** MIDAS TEC map for 29 October 2003 at 19:00 UT h

Fig1

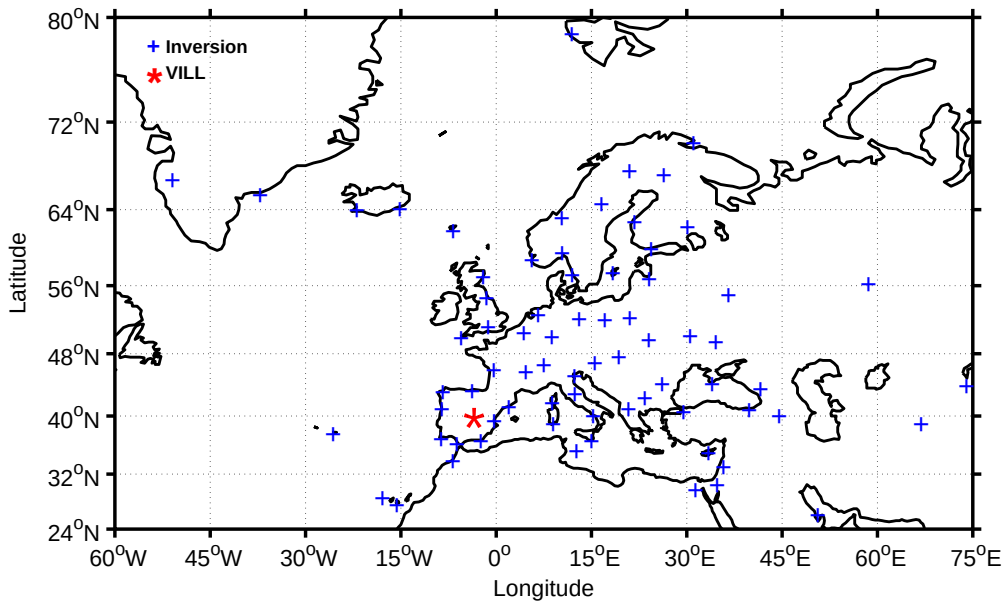
Inversion
VILL
80°N
72°N
64°N
56°N
48°N
40°N
32°N
24°N
Latitude
60°W
45°W
30°W
15°W
0°
15°E
30°E
45°E
60°E
75°E
Longitude

Fig2a

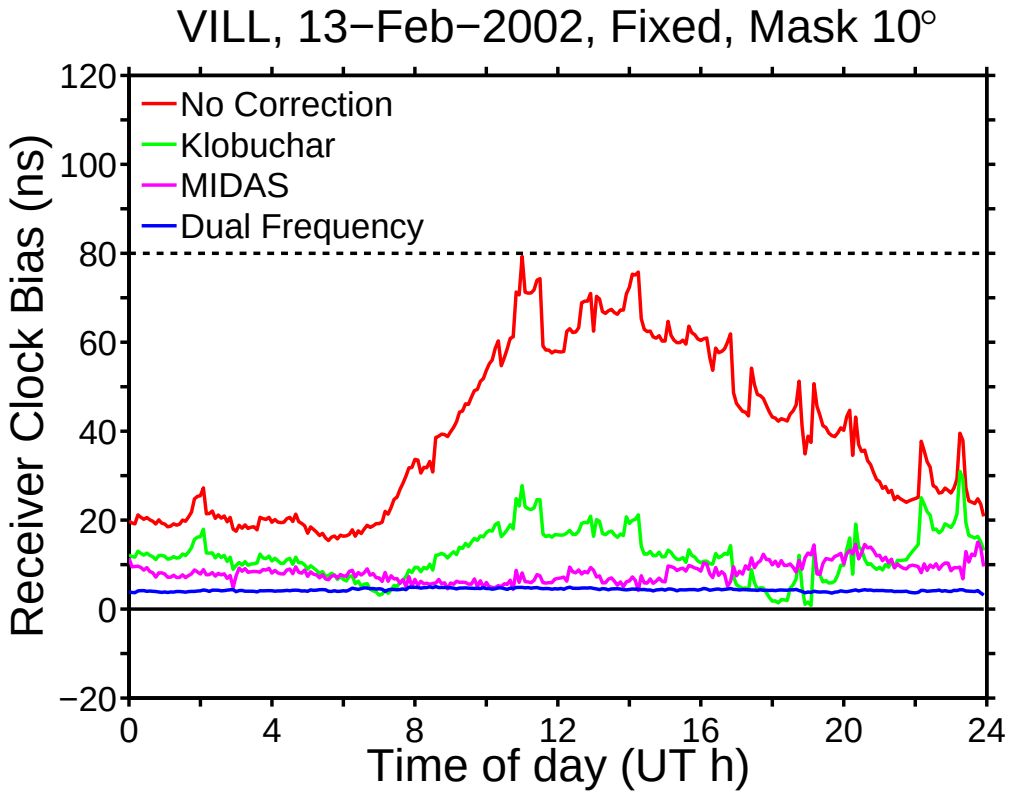
VILL, 13−Feb−2002, Fixed, Mask 10°
No Correction
Klobuchar
MIDAS
Dual Frequency
Receiver Clock Bias (ns)
120
100
80
60
40
20
0
−20
0
4
8
12
16
20
24
Time of day (UT h)

Fig2b

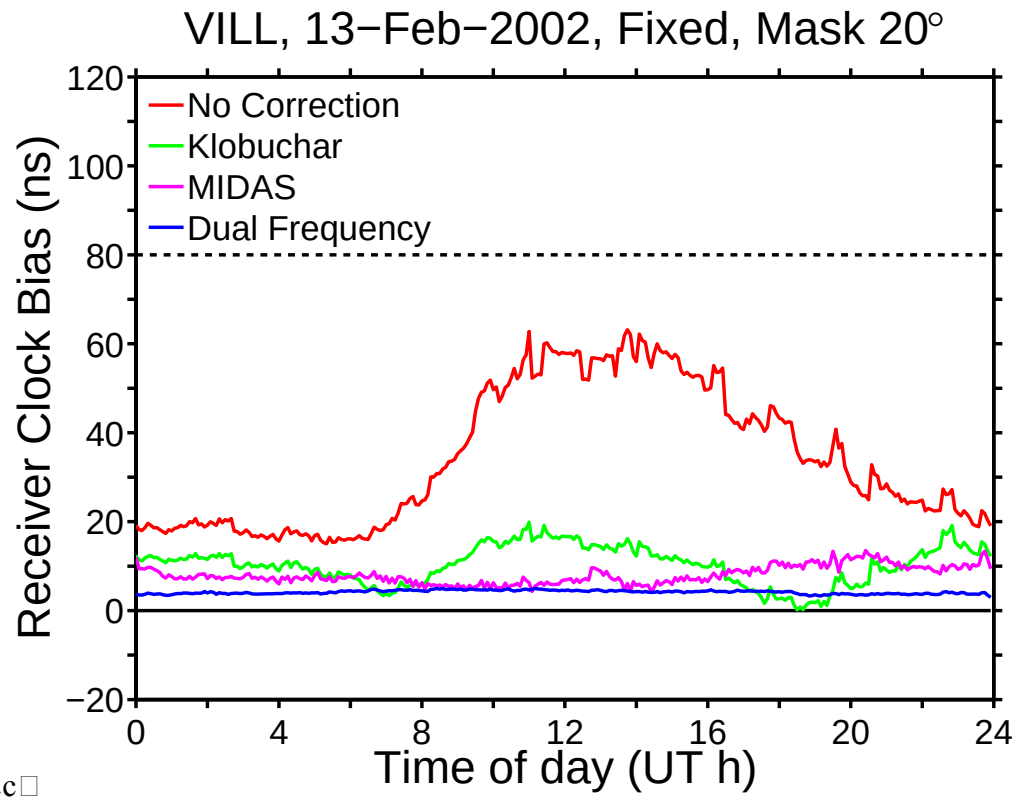
VILL, 13−Feb−2002, Fixed, Mask 20°
No Correction
Klobuchar
MIDAS
Dual Frequency
Receiver Clock Bias (ns)
Time of day (UT h)
120
100
80
60
40
20
0
−20
0
4
8
12
16
20
24

Fig2c

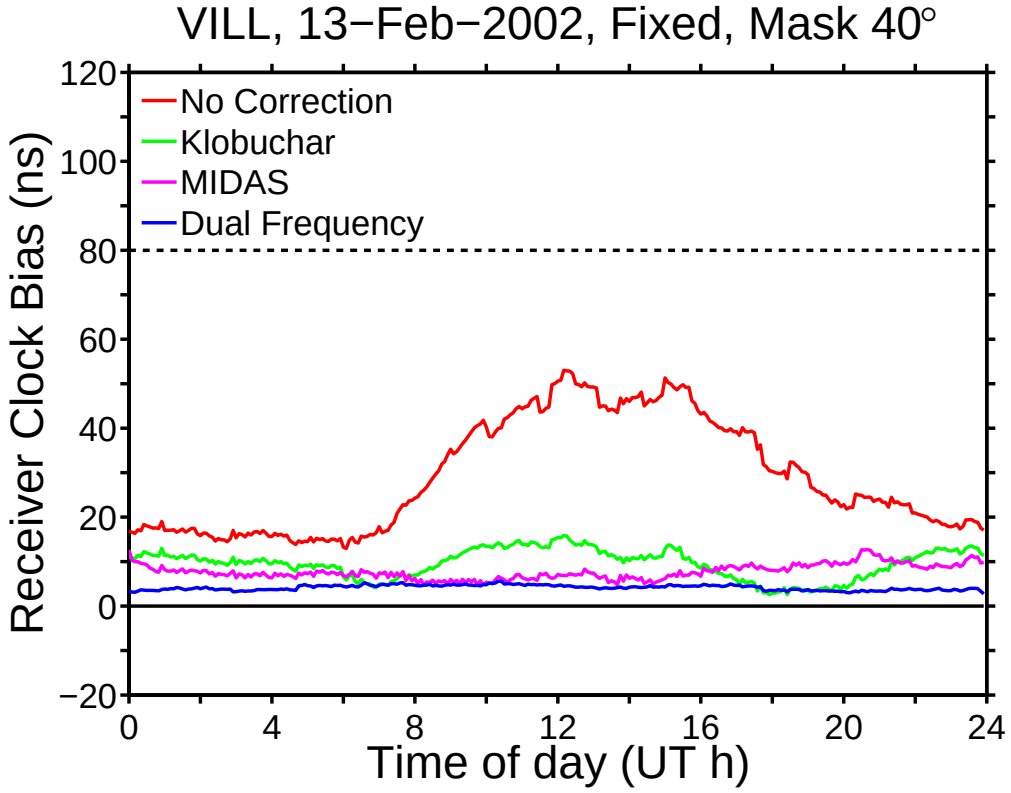
VILL, 13−Feb−2002, Fixed, Mask 40°
No Correction
Klobuchar
MIDAS
Dual Frequency
Receiver Clock Bias (ns)
Time of day (UT h)
120
100
80
60
40
20
0
−20
0
4
8
12
16
20
24

Fig3a

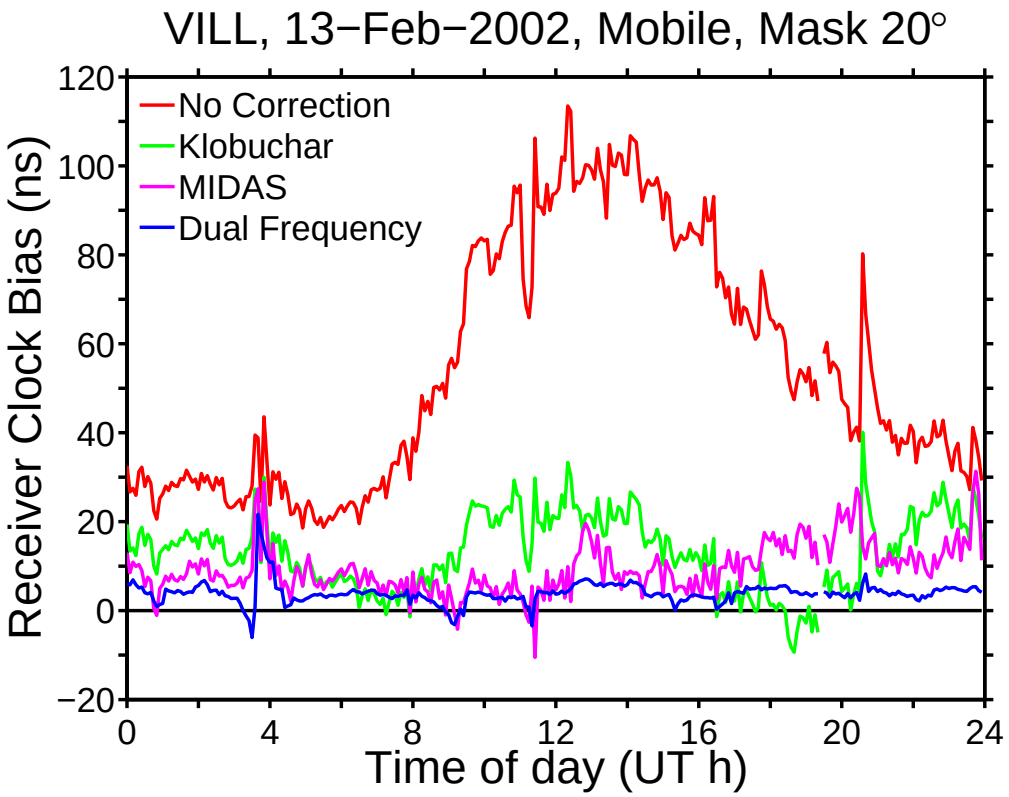
VILL, 13−Feb−2002, Mobile, Mask 20°
No Correction
Klobuchar
MIDAS
Dual Frequency
Receiver Clock Bias (ns)
120
100
80
60
40
20
0
−20
0
4
8
12
16
20
24
Time of day (UT h)

Fig3b

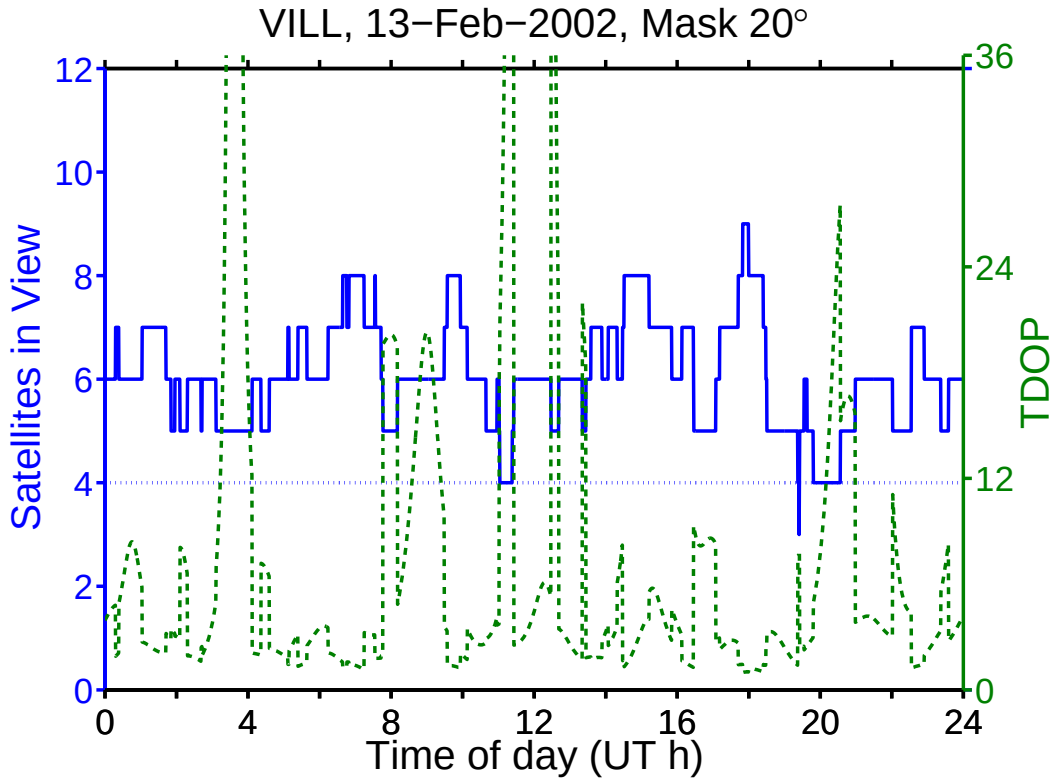
VILL, 13−Feb−2002, Mask 20°
Satellites in View
TDOP
12
10
8
6
4
2
0
36
24
12
0
0
4
8
12
16
20
24
Time of day (UT h)

Fig3c

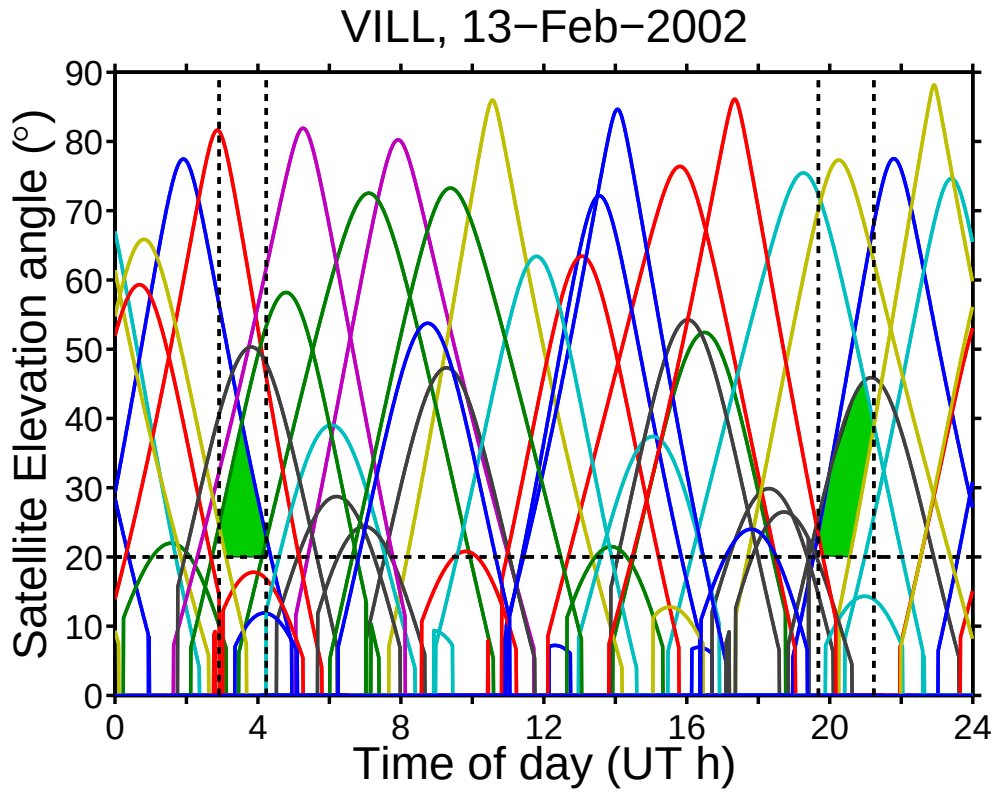
VILL, 13−Feb−2002
Satellite Elevation angle (°)
Time of day (UT h)
0
10
20
30
40
50
60
70
80
90
0
4
8
12
16
20
24

Fig3d

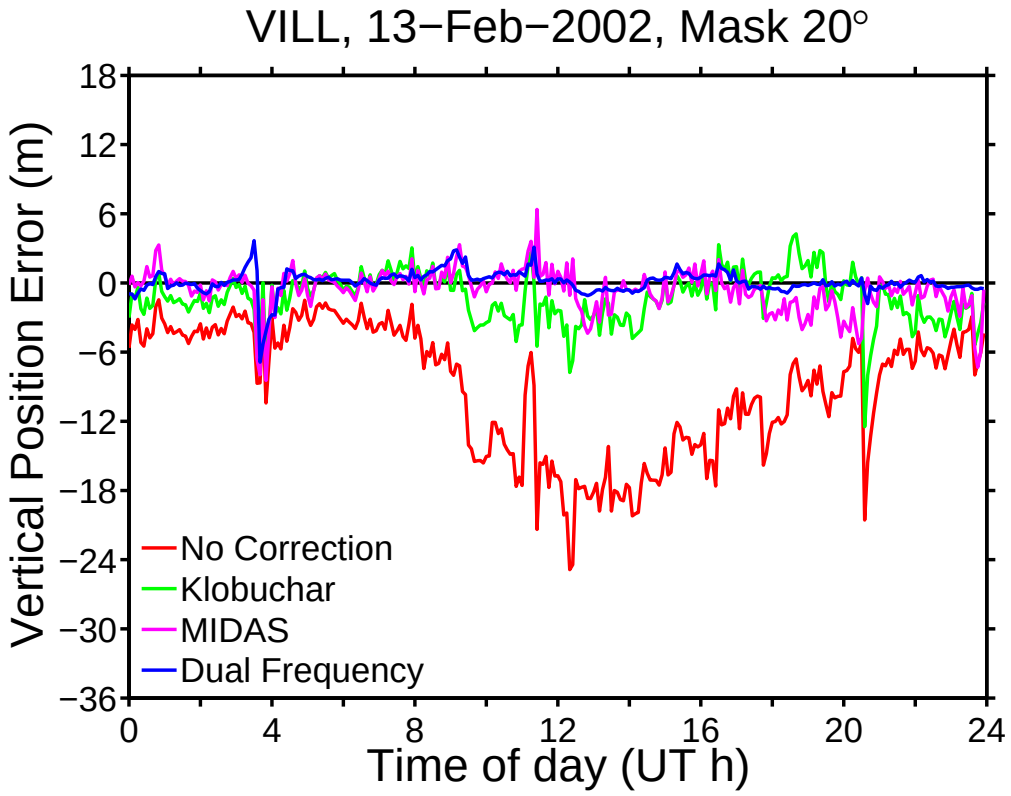
VILL, 13−Feb−2002, Mask 20°
Vertical Position Error (m)
Time of day (UT h)
No Correction
Klobuchar
MIDAS
Dual Frequency
18
12
6
0
−6
−12
−18
−24
−30
−36
0
4
8
12
16
20
24

Fig3e

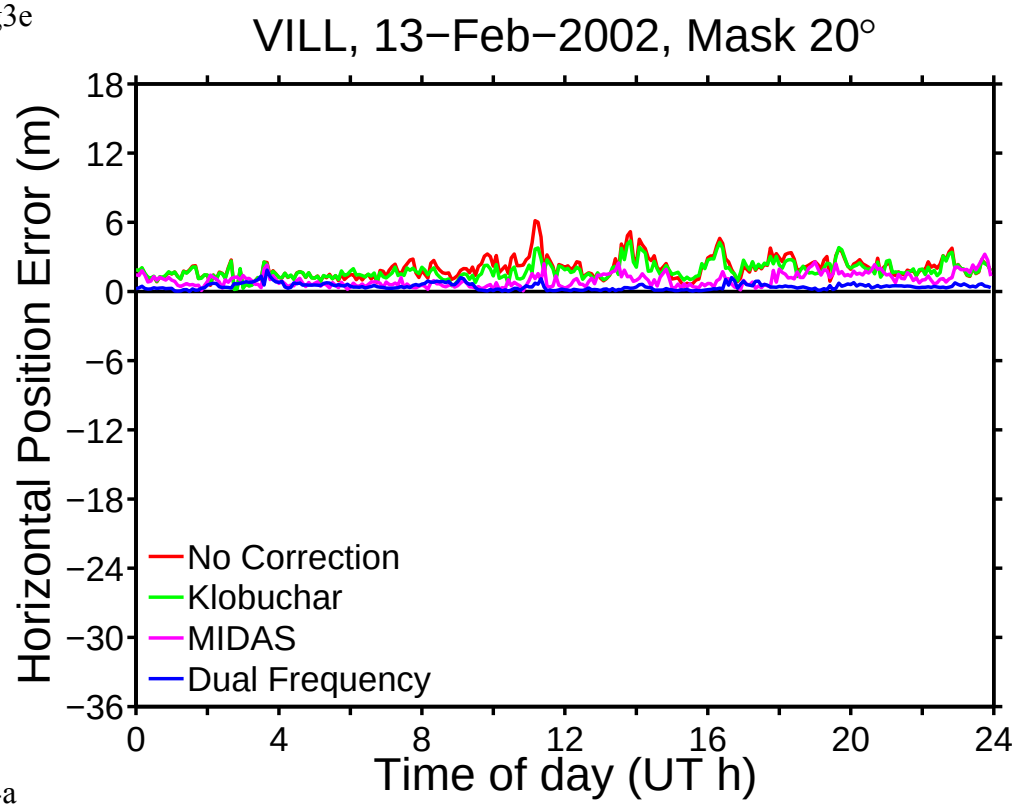
VILL, 13−Feb−2002, Mask 20°
Horizontal Position Error (m)
18
12
6
0
−6
−12
−18
−24
−30
−36
No Correction
Klobuchar
MIDAS
Dual Frequency
0
4
8
12
16
20
24
Time of day (UT h)

Fig4a

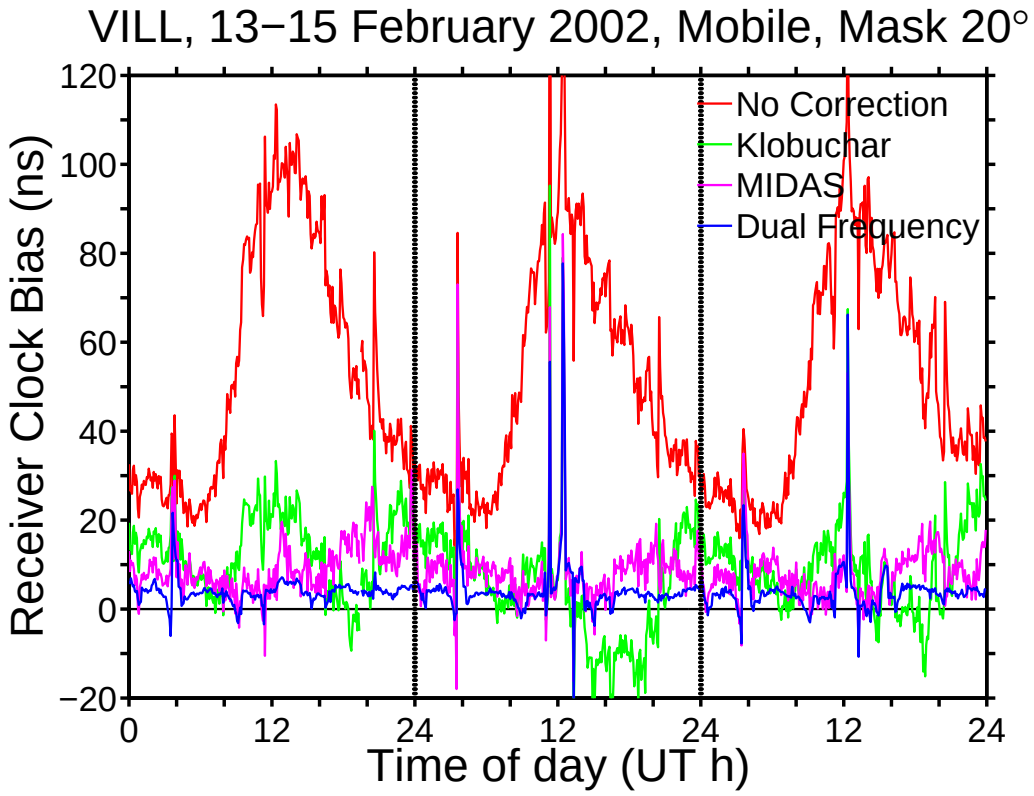
VILL, 13−15 February 2002, Mobile, Mask 20°
Receiver Clock Bias (ns)
120
100
80
60
40
20
0
−20
No Correction
Klobuchar
MIDAS
Dual Frequency
0
12
24
12
24
12
24
Time of day (UT h)

Fig4b

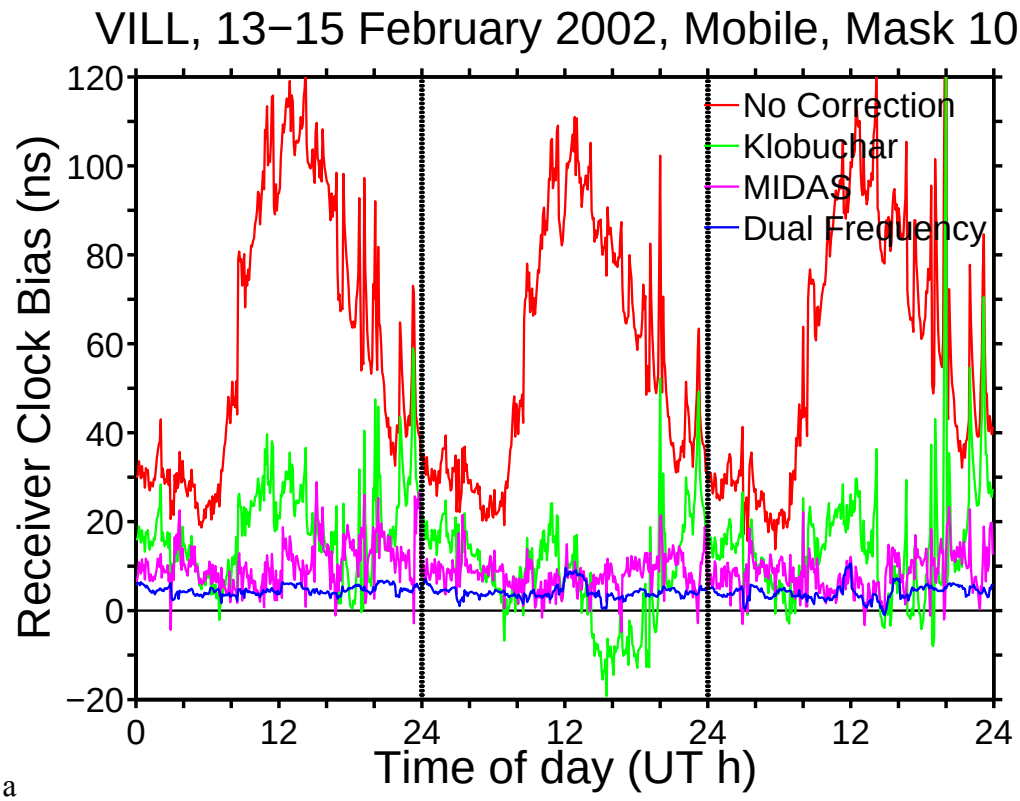
VILL, 13−15 February 2002, Mobile, Mask 10°
Receiver Clock Bias (ns)
Time of day (UT h)
No Correction
Klobuchar
MIDAS
Dual Frequency
120
100
80
60
40
20
0
−20
0
12
24
12
24
12
24

Fig5a

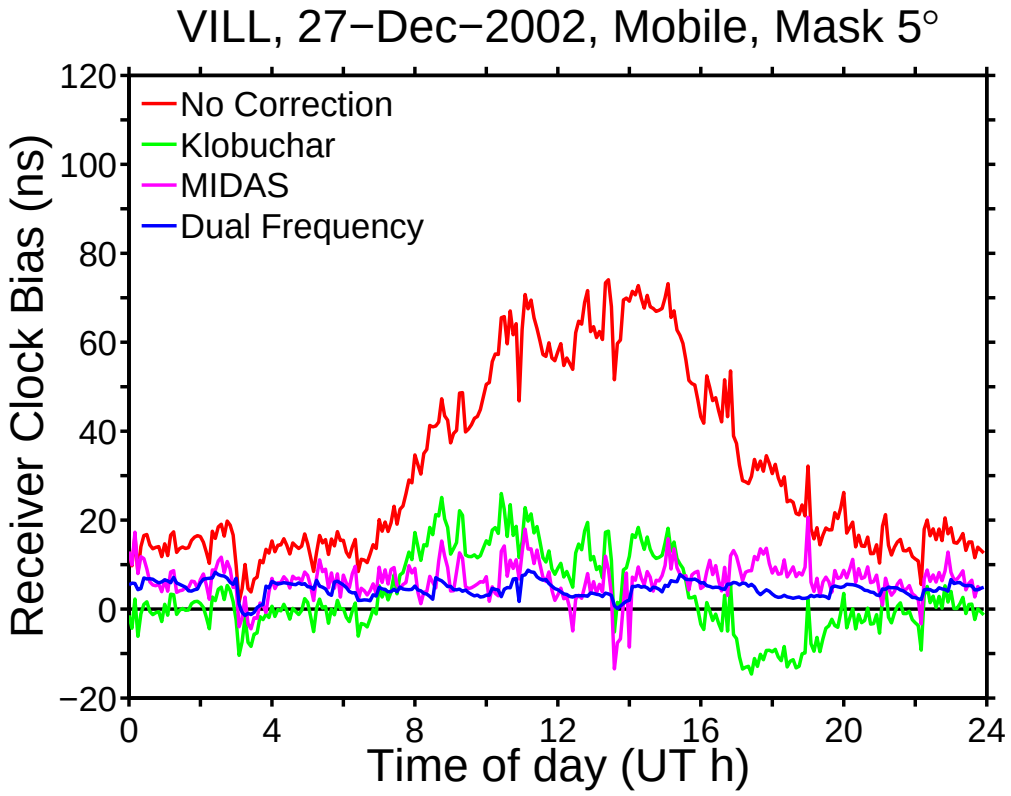
VILL, 27−Dec−2002, Mobile, Mask 5°
Receiver Clock Bias (ns)
Time of day (UT h)
No Correction
Klobuchar
MIDAS
Dual Frequency
120
100
80
60
40
20
0
−20
0
4
8
12
16
20
24

Fig5b

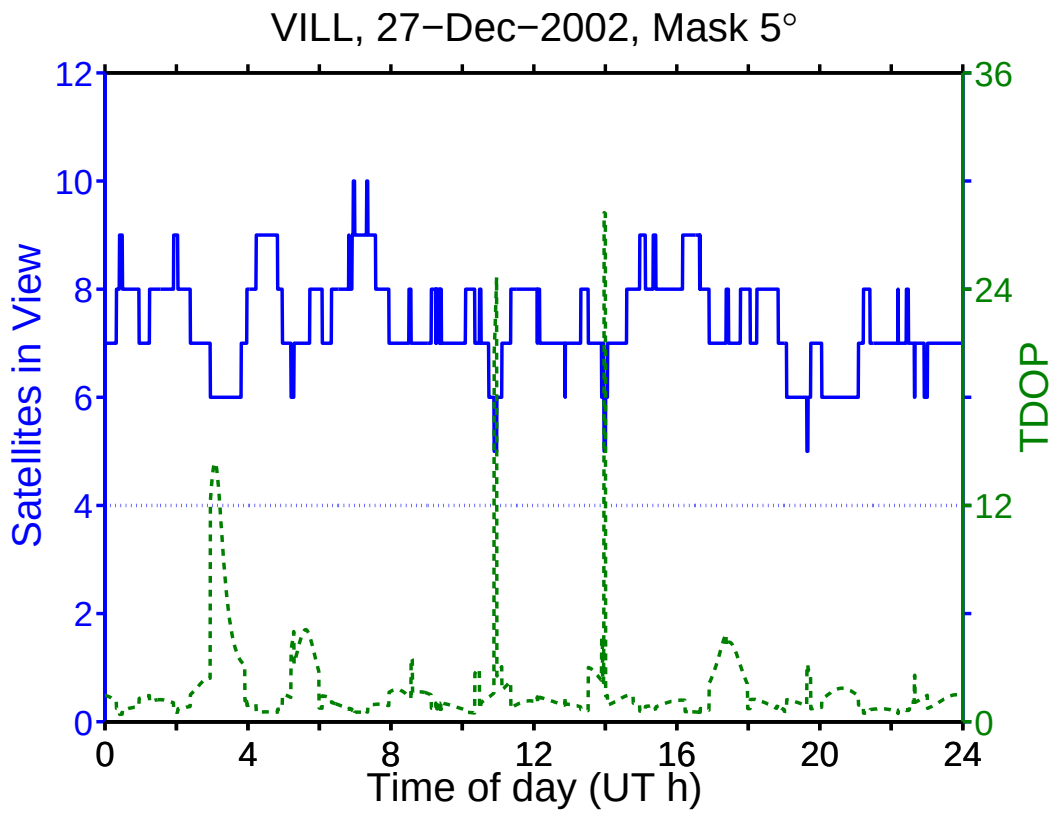
VILL, 27−Dec−2002, Mask 5°
Satellites in View
TDOP
Time of day (UT h)
0
2
4
6
8
10
12
0
12
24
36
0
4
8
12
16
20
24

Fig5c

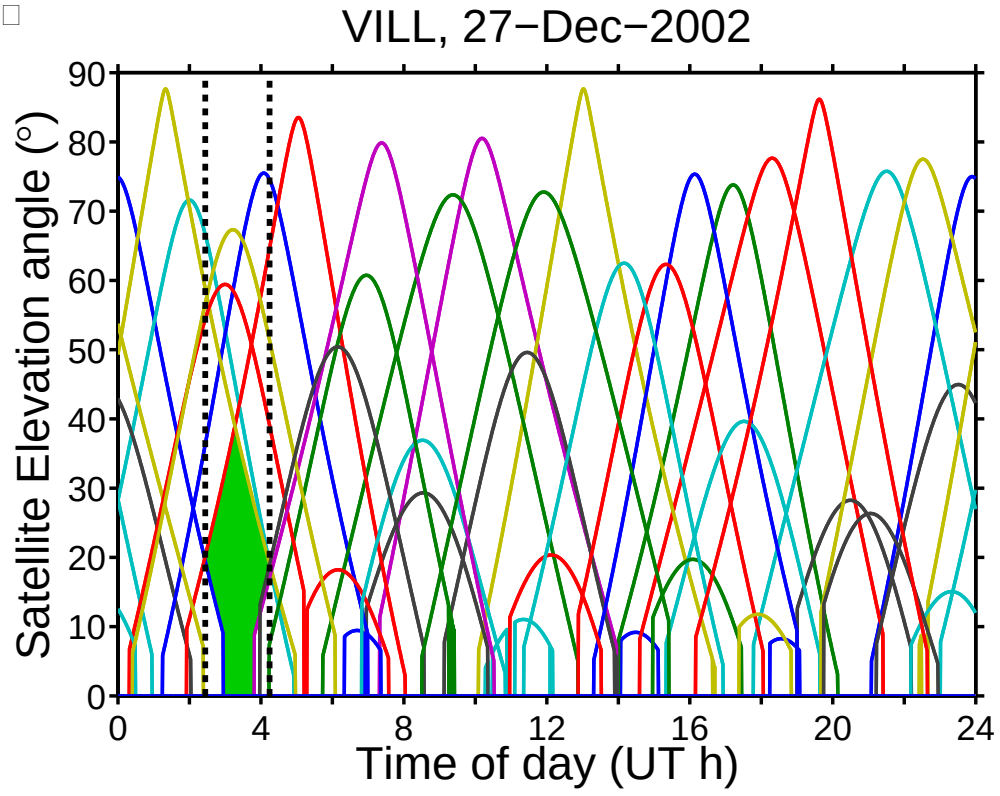
VILL, 27−Dec−2002
Satellite Elevation angle (°)
Time of day (UT h)
0
10
20
30
40
50
60
70
80
90
0
4
8
12
16
20
24

Fig6a

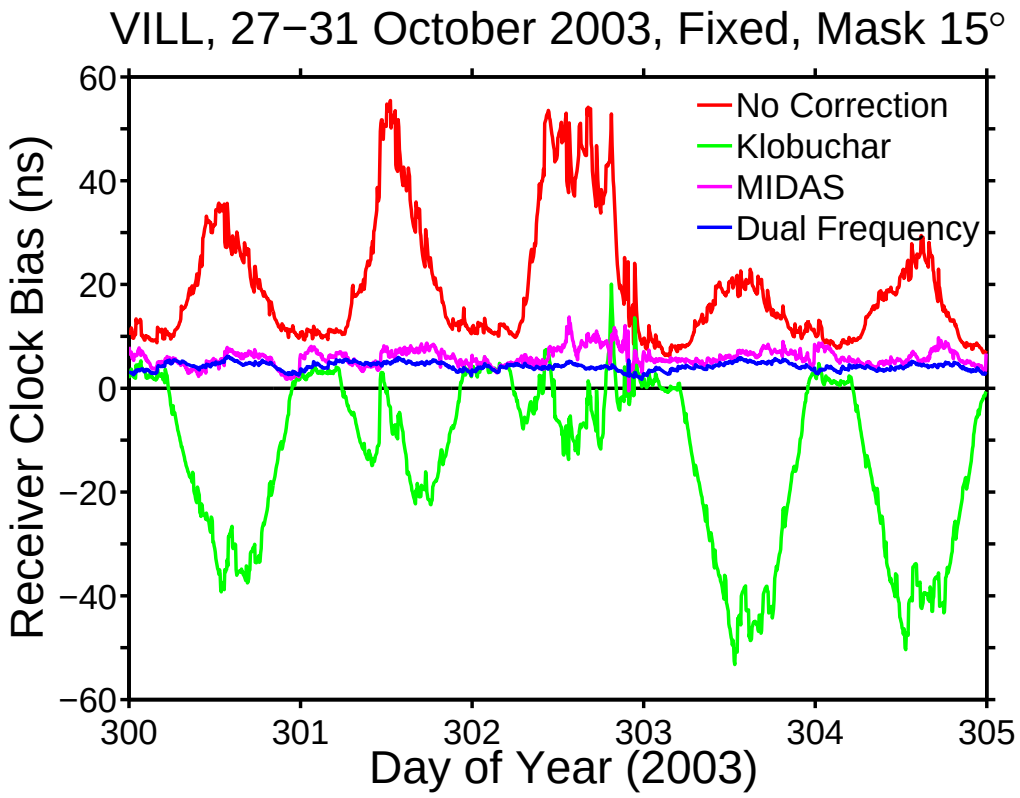
VILL, 27−31 October 2003, Fixed, Mask 15°
No Correction
Klobuchar
MIDAS
Dual Frequency
Receiver Clock Bias (ns)
60
40
20
0
−20
−40
−60
300
301
302
303
304
305
Day of Year (2003)

Fig6b

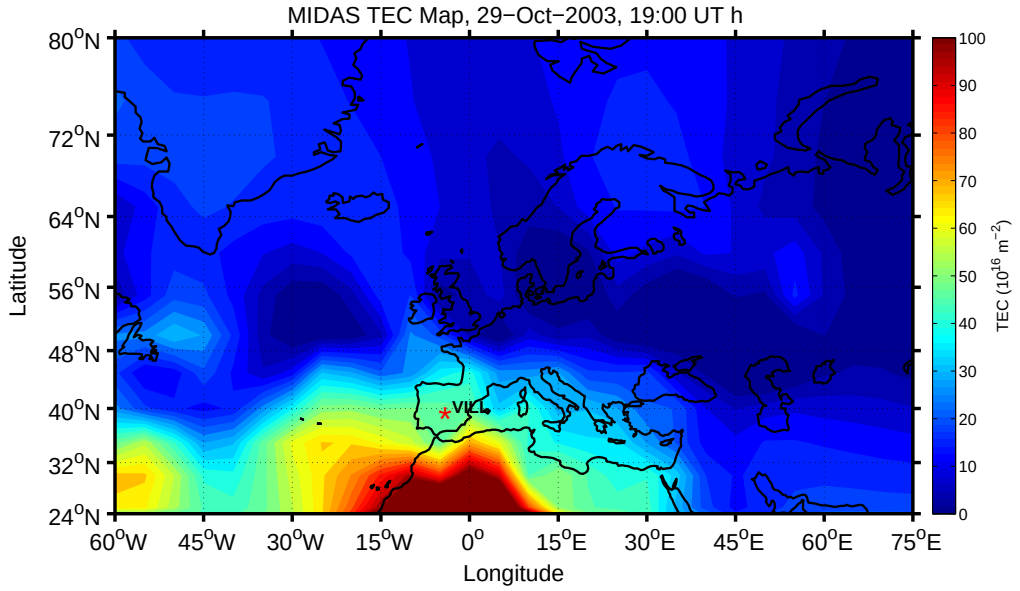
MIDAS TEC Map, 29−Oct−2003, 19:00 UT h
80°N
72°N
64°N
56°N
48°N
40°N
32°N
24°N
Latitude
VILL
60°W
45°W
30°W
15°W
0°
15°E
30°E
45°E
60°E
75°E
Longitude
100
90
80
70
60
50
40
30
20
10
0
TEC (10^16 m^-2)

Table 1 RMS receiver clock bias (ns) referenced to the receiver clock bias from CODE (using the fixed receiver solution at VILL) with 5°, 15°, 20° and 40° elevation masks, for geophysically quiet and stormy days selected from each month of 2002, excluding September due to data quality.

GPS Timing Solution	RMS receiver clock bias (ns)			
	5° mask	15° mask	20° mask	40° mask
No correction	34.9	30.8	28.9	24.4
Klobuchar	11.0	9.4	8.8	7.8
MIDAS	6.7	6.3	6.3	6.1
Dual-frequency	4.4	4.3	4.3	4.2

Table 2 Standard deviation (ns) (using the fixed receiver solution at VILL) with 5°, 15°, 20° and 40° elevation masks, for geophysically quiet and stormy days selected from each month of 2002, excluding September due to data quality.

GPS Timing Solution	Standard deviation of the receiver clock biases (ns)			
	5° mask	15° mask	20° mask	40° mask
No correction	15.3	13.1	12	9.7
Klobuchar	8.9	7.8	7.3	6.2
MIDAS	2.2	2.1	2.1	2.0
Dual-frequency	1.8	2.0	2.0	1.7

Table 3 RMS receiver clock bias (ns) referenced to the receiver clock bias from CODE (using the fixed receiver solution at VILL) with 5°, 15°, 20° and 40° elevation masks, calculated over a geophysically stormy period between 27-31 October 2003.

GPS Timing Solution	RMS receiver clock bias (ns)			
	5° mask	15° mask	20° mask	40° mask
No correction	25.2	22.8	21.4	18.1
Klobuchar	22.5	20.7	19.5	15.2
MIDAS	6.3	6.1	6.1	5.9
Dual-frequency	4.4	4.3	4.2	4.2

Table 4 Standard deviation (ns) (using the fixed receiver solution at VILL) with 5°, 15°, 20° and 40° elevation masks, calculated over a geophysically stormy period between 27-31 October 2003.

GPS Timing Solution	Standard deviation of the receiver clock biases (ns)			
	5° mask	15° mask	20° mask	40° mask
No correction	13.1	11.9	11	8.9
Klobuchar	17.3	16.0	15	11.9
MIDAS	1.8	1.6	1.6	1.6
Dual-frequency	0.7	0.8	0.8	0.9